UNIVERSITY OF CALIFORNIA, IRVINE

Visualization of Classical and Relativistic Spacetime Geometry

THESIS

Submitted in partial satisfaction of the requirements for the degree of

MASTER OF SCIENCE

in Information and Computer Science

by

Don V. Black

Thesis Committee:
Research Physicist Frank Wessel
Associate Professor Renato Pajarola
Associate Professor James Arvo
Assistant Professor Falko Kuester, Co-Chair
Assistant Professor Gopi Meenakshisundaram, Chair

2005

The thesis of Don V. Black is approved:

_____

_____

_____

_____

_____

Committee Chair

University of California, Irvine
2005

DEDICATION

For my beloved wife, Noel, who gave me the space and time to grow.

TABLE OF CONTENTS

List of Figures

ACKNOWLEDGEMENTS

My thanks to Dr Arvind Rajaraman of the UCI Department of Physics and Astronomy for lending his unique expertise, and to Dr Ron Stern, Dean of the School of Physical Sciences, for his help and suggestions. A special thanks to Dr James Arvo of the UCI Donald Bren School of Information and Computer Sciences for providing the source code of his ToyTracer raytrace kernel. A very great thank-you to Dr Falko Kuester for his advice and support, but mostly for his engineer's tenacity and commitment to see this project through.

ABSTRACT OF THE THESIS

Visualization of Classical and Relativistic Spacetime Geometry

by

Don V. Black

Master Of Science In Information and Computer Science

University of California, Irvine, 2005

Recent advances in physics have suggested new physical models that incorporate multiple spatial dimensions to explain new cosmological evidence. These new theories are a challenge to envision and difficult to grasp. Adapting visualization algorithms and strategies to the new physics of multiple dimensions can aid in understanding these non-intuitive phenomena.

Presented here is an adaptation of 4D ray tracing to a spacetime model that captures Einsteins geometry and shows how relativistic phenomena such as Terrell rotation, aberration, retarded time and even animation and motion blur, can emerge from a static spacetime model. This technique has made it possible to explore the fundamental nature of Einsteins geometric model by decoupling finite light-speed from time dilation and length contraction.

The geometry of a toy four-dimensional spacetime model is examined and viewed. First, expected special relativistic visual effects are defined, as are the contemporary methods to visualize these relativistic effects. Next, one visualization method is selected, along with one spacetime model, and a set of expected visual geometric effects. Images and animations of these expected visual effects are then generated, displayed, and measured, thus demonstrating that the selected spacetime model conforms to expected relativistic effects.

Chapter 1

Introduction

The intent of this thesis is to identify an accurate method to visualize spacetime, and in the process reveal unexpected and heretofore unknown relationships among physical phenomena. In order to achieve this goal the simplest of possible models of four-dimensional spacetime will be devised and graphically visualized via animation.

The fields of spacetime physics, four-dimensional visualization, and relativistic visualization will be researched. A geometric model will be selected that most favorably reflects the underlying principles of special relativity and the geometry of spacetime.

The theoretical background of special relativity will be discussed first. Next, contemporary four-dimensional and special relativistic visualization strategies will be examined. Then the visual effects that are expected will be identified. From these latter effects test cases will be selected. From the strategies a model and a method will be selected and implemented.

The model will be tested against the expected visual effects, and conclusions will be drawn.

1.1 Background

At the time of Einstein's discovery of relativity [17], Maxwell's equations [35] were known, and the speed-of-light (c) was being measured [48] with some accuracy. The theoretical physicists of the time were considering the physical implications of such a speed limit to the laws of the Universe.

This is when Einstein (Timeline [9]) departed from convention and suggested that the speed-of-light was constant but time varied (rather than vice-versa). This concept had profound implications on the meaning of causality and simultaneity. The 'future' was no longer easily distinguishable from the 'past' - it was possible for a space-time event to be neither future nor past. As proposed by Poincare [43], H. G Wells [57], and Minkowski [36], Einstein's Theory of Relativity incorporated the concept of time as another dimension for a heretofore three-dimensional Universe.

1.2 Einstein's Two Theories of Relativity

Einstein's Theory of Relativity was developed in two stages: Special Relativity [17] and General Relativity [18]. As the names suggest, Special Relativity (or **SR**) deals with the ***special case*** of relativity where the Universe (locally) is empty of mass and space is 'flat'. In **SR** there is no gravitational curvature and light always travels in a straight line, as does a mass at a constant velocity. General Relativity (or **GR**) on the other hand deals with the ***general case*** where space may be either flat or curved. In **GR** there may be gravitational curvature so that light rays can bend while traversing space. The Special Theory (**SR**) is a special case or subset of the General Theory (**GR**). (Do not confuse acceleration, per se, which can exist in **SR**, with acceleration due to gravitational curvature which can exist only in **GR**).

Both these theories have the following two postulates of Einstein in common:

1. **The Relativity Postulate:** The laws of physics are the same for observers in all inertial frames[1]. No one frame is a preferred frame.
2. **The Speed of Light Postulate:** The speed of light in vacuum has the same value (c) in all directions and in all inertial frames.

Any observer traveling at any velocity will measure the speed-of-light in a vacuum to be the same, approximately 3×10^8 m/s. In a Euclidean three-dimensional space, these postulates require both length-contraction and time-dilation for consistency with observed phenomena [19]. That is to say, two different observers traveling at different velocities will measure the other observer's meter-stick as shorter and the other observer's clock as slower than their own. Experiment has shown this to be true, both directly and indirectly.

For such a phenomena, there can be only one invariant lightspeed [47]. Einstein picked a Lorentz transform such that the speed of light (c) was finite and invariant. This implies that the propagation of all causality must be limited to lightspeed. This includes all information about the local state of the Universe such as gravity, energy, force, mass, etc. If so, the speed-of-gravity must likewise be equal to c. As of this writing, experimentation is in progress to determine if this is indeed true. This is all very different from day-to-day experiences, that is to say, it is nonintuitive.

For a definitive treatment of Einstein's Theory of Special Relativity, the reader is directed to the physics literature [18][36][11][46].

1.3 Extra Dimensions

> "Henceforth space by itself, and time by itself, are doomed to fade away into mere shadows, and only a kind of union of the two will preserve an independent reality." - Hermann Minkowski (1908)

Minkowski [36] defined four-dimensional spacetime as three-dimensional space with an orthogonal one-dimensional time axis. The time dimension has different characteris-

[1]The term ***inertial reference frame*** (***IRF***) refers to a coordinate system that is either at rest or is moving in a straight line with a constant velocity. Any object or observer in an inertial reference frame experiences no unbalanced forces and is not accelerating (Newton's First Law).

tics than the 3 space dimensions. This space-time is referred to as ***3+1*** dimensionality: 3 isotropic spatial dimensions plus 1 anisotropic temporal dimension.

In 1914, still before the discovery of General Relativity, Nordstrom [37] attempted to unify gravity and electromagnetism in a five-dimensional flat space-time. In the wake of Einstein's General relativity, Theodor Kaluza [31] extended GR into five-dimensions and attempted to extract ordinary four-dimensional Einstein gravity and Maxwell electromagnetism [35]. According to Appelquist [2], Einstein refereed Kaluza's paper and approved it in 1921, when Oskar Klein [32] specified that the extra dimension's size was on the order of the Planck length (10^{-35}m). Since that time, String Theories have been built on the **Kaluza-Klein Theories** [2] to suggest 10, 11 and 26 dimensions of various sizes and characteristics.

The latest theories suggest that the three-dimensional Universe is but one three- or four-dimensional membrane (*brane*) in a higher dimensional *bulk* universe, similar to one of the many two-dimensional walls in a three-dimensional house.

Chapter 2

Theory

2.1 The Spacetime Model

Einstein's four-dimensional spacetime (t,x,y,z) model consisting of both space and time, is often referred to as (3+1)D, that is, three isotropic spatial dimensions (x,y,z) and one anisotropic time dimension (t). This convention will be used throughout this document.

A four-dimensional spacetime point (t,x,y,z) will be referred to as an ***event***.

It is assumed that spacetime is flat. The path of a lightray is therefore a straight line, as is the path of an object with a constant velocity. All objects treated herein shall have a constant velocity.

The camera will lie on the t axis, thus its spatial components will always be zeros: $(t,0,0,0)$. The terms camera and point-of-view (POV) may be used interchangeably. (Purists may wish to conceptualize a pin-hole camera that does *not* invert the image, with the pin-hole at the point-of-view [23].)

For this discussion the camera frame's three-dimensional axes will be rotated such that the x axis is parallel with the object's velocity vector, so $\Delta z = \Delta y = 0$. Speed will be measured as a fraction ($\beta = \frac{v}{c}$) of lightspeed (c).

The ***worldline*** of an object marks the object's path through four-space from event to event. An object whose worldline is parallel to the camera's t (time) axis is stationary in the camera frame, since $\Delta x = 0$, $v = \frac{\Delta x}{\Delta t} = 0$. Conversely, an object whose worldline is not parallel to the camera's t axis has a velocity with respect to the camera, since $\Delta x \neq 0$. The ***worldlines*** of all objects treated herein shall be straight lines.

The normalized instantaneous tangent of the worldline of an object in the camera frame is the object's normalized velocity four-vector (τ) in the camera frame. In the object's rest frame, this velocity four-vector is also the ***proper*** time (t) axis for the **inertial reference frame** in which the object is at rest (the object frame). For an object with a constant velocity (no acceleration) in an inertial reference frame, the worldline and the velocity four-vector for that object are collinear. The velocity of an object in the camera frame is a monotonically increasing function with respect to the angle between the object's velocity four-vector (worldline) and the time axis of the camera frame.

Temporal extrusion is the construction of a higher-order (n-D) object by extruding its lower-order ($(n-1)$-D) counterpart along its velocity four-vector, and connecting its

respective bounding $(n-2)$-D simplices to create $(n-1)$-D simplices bounding the higher-order object. For example, a prism could be created by extruding a triangle parallel to the triangle's t axis.

The operation optionally includes applying a Lorentz transform to objects whose extrusion angles are not parallel to the camera (laboratory) frame's time axis. A ***Lorentz-decoupled*** (or classical) object is one which was inserted into the scene without the Lorentz transform (an unphysical object).

Planck or natural units, which are unitless ($c = 1$), will be used throughout this document for convenience. The benefit of natural units is that the units of measure along all the spacetime axes are similar, i.e. the t axis as well as the x, y, and z axes have the same scale and identical units of measure.

This is equivalent to stating that the t axis has been scaled by c (speed-of-light), yielding a ct axis. A lightray will travel one unit (of Euclidean distance) along the spatial axes for each unit it travels along the time axis - the lightrays always bisect the angle between the time axis and the 3 spatial axes. In other words, the t component of the normalized lightray direction four-vector should always be $-\frac{\sqrt{2}}{2}$. Furthermore, the lightrays lie on the hypersurface of a bisecting hypercone (depicted in Figure 4.2) whose apex is at the origin and whose symmetric axis is collinear with the negative time axis. In other words, the traced rays always lie at 45° to the $-t$ axis.

By convention, the term ***relativistic velocity*** will be used to describe the relative speeds between the two referents of approximately 0.866 of lightspeed ($0.866c$) or greater. In some cases the term ***relativistic*** is used as a modifier to describe an object that is moving with relativistic velocity with respect to the camera frame or a referent observer.

2.2 Expected Visual Effects

There are certain visual effects that must be accounted for by any relativistic visualization technology. These effects include geometric distortions as well as changes in brightness, viewing directions, and color. The optimal algorithm would accommodate all these phenomena without special consideration. The best technique may also yield new and unexpected results.

Rather than treat the effects of relativistic velocities, the fundamental nature of spacetime that causes the relativistic effects will be addressed. The visual effects of relativistic motion are divided into two categories: ***relativistic phenomena*** that are a result of the fundamental nature of three-space; and ***classical phenomena*** due to viewing three-space with a finite lightspeed. In the relativistic category are length contraction and time dilation. In the later classical category are visual effects such as retarded time and classical aberration. Relativistic aberration, Terrell rotation, and Doppler shift are due to both relativistic and classical contributions.

Throughout this document the term ***inertial reference frame*** (***IRF***) will be used to refer to a coordinate system that is either at rest or is moving in a straight line with a constant velocity. Any object or observer in an inertial reference frame is not accelerating. In the following discussion, it is assumed that the observer (the camera), unless explicitly stated otherwise, is at rest in the laboratory inertial reference frame. Relativistic objects are

moving in their own inertial reference frames at relativistic velocities with respect to the laboratory or camera frame.

2.2.1 Geometric Distortion

As noted above, ***classical*** distortion is due to a finite light speed. Any light speed, e.g. 30 km/h or $3 * 10^8$ m/s, would cause visual distortion[1], due to the delay in delivering information from different parts of the object. However, ***relativistic*** distortions are fundamental characteristics of the spacetime continuum, not merely 'apparent'. In this category are length contraction and time dilation.

Length Contraction

Length contraction in the direction of travel is a fundamental property of the physics of the three-dimensional Universe. Length contraction is not a classic effect resulting from the finite speed of light, but is as 'real' as mass and momentum. While it may be difficult to extrapolate from three-dimensions what is 'real' in four-dimensions, it is possible to construct a self-consistent four-dimensional model that yields empirical results consistent with observations within three-dimensions.

Length contraction of a moving object is a phenomenon that can be modeled by three spatial dimensions embedded in a four dimensional spacetime [42]. For an object with a constant velocity, the object's dimensions in four-space remain constant. The length contraction can be considered to be the projection of a three-dimensional cross section of the static four-dimensional object orthogonal to the observer's time axis. While this phenomenon can be considered an illusion from the point-of-view of a four-dimensional observer, it is a 'real' and measurable physical phenomena to a three-dimensional observer.

The effect becomes more apparent as the relative velocity of an object approaches the speed of light. For example, at 86.6% of the speed of light, an object shrinks to $\frac{1}{2}$ its rest (or proper) length. Change of velocity changes the t axis and so changes the projection angle. As the velocity increases, the projected angle changes and so reduces the length in the direction of motion.

Terrell Rotation

Terrell rotation is an effect of light's finite speed complementing the effect of length contraction. From the point of view of an observer at rest, proximate surfaces of a relativistically moving object appear to rotate so that the surfaces facing the observer will face the direction of motion, and distant hidden surfaces become visible. This is the result of a finite lightspeed, where light from the more distant surfaces carry information about where the object was further in the past than the light from the proximate surfaces.

Consequently, when a spherical object moves past an observer, the observer can 'see' both the front and part of the back of the relativistic sphere. At a relative velocity near to the speed-of-light the sphere will appear to have rotated nearly 90 degrees such that the

[1] George Gamow [22] presents a charming description of relativistic effects through the eyes of Mr. Tompkins, who rides his bicycle in a world where lightspeed is only 30 km/h.

trailing quarter of the sphere opposite the observer is visible to the observer. The apparent rotation of the sphere and the retarded light signal conspire to ensure that the silhouette of the sphere remains circular. This effect can be seen in Figure 2.1 and the accompanying animations [9]. Note that while the silhouette of the relativistic sphere remains circular, the surface texture has distorted such that it appears to have rotated forward about a vertical axis perpendicular to the view vector and the velocity vector as predicted.

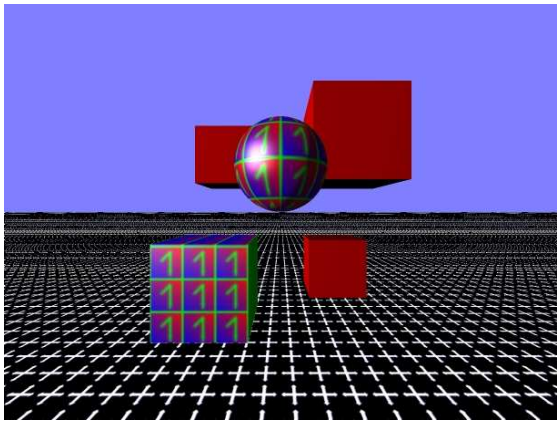

Figure 2.1: View of stationary sphere & 4 cubes.

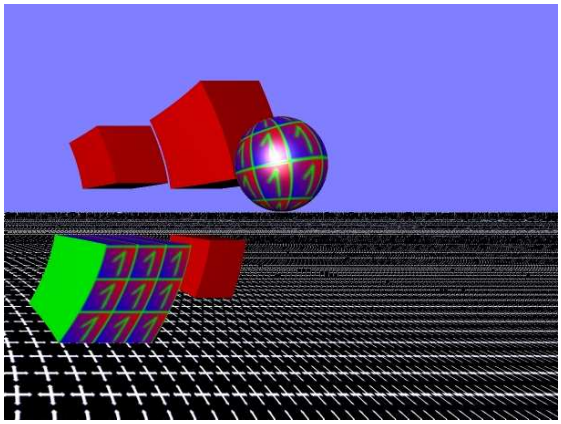

Figure 2.2: View of sphere & 4 cubes moving left to right past camera.

2.2.2 Aberration

Just as when an automobile speeds along through a gentle rain, and the falling rain seems to stream from front to back, so light's photons seem to stream from front to back as a rocket moves forward relativistically past a star. This effect is 'aberration'. The faster the rocket, the more that the star seems to migrate to the front of the rocket. While counter-intuitive, this can be demonstrated with simple vector addition as shown in Section 2.3.2, Classical Aberration. But vector addition is not the whole story, since relativistic velocities are involved, as described in Section 2.3.3.

2.2.3 Intensity & Color

Searchlight Effect

A relativistic observer will experience an increased light intensity coming from the forward direction along the velocity vector. Intensity is the radiant energy (photons) per unit area per unit time. The searchlight effect is an increase in the intensity as a result of a combination of aberration and time dilation. As the velocity of an observer relative to an emissive surface (e.g. - a star) increases, the number of photons encountered by the observer per unit time increases. The observer's increased velocity will also increase the aberration effect, causing more of the light emitting surface to migrate towards the direction of motion, thus increasing the light density in front of the observer. More photons more often means brighter light.

However, as the emitting surface's time dilates with respect to the observer, less radiant energy (fewer photons) are emitted per unit time. This marginally reduces the intensity due to the searchlight effect. But there is still a net gain in intensity. The wavelength of the incident photons also length contract (yielding a higher frequency or greater energy). This effect is discussed below in Section 2.2.3.

Doppler Shift

The change in the apparent frequency (color) of a lightray is attributed to the relativistic Doppler shift. This is a combination of the classic Doppler shift with the added relativistic contribution of length contraction and time dilation. As with sound in air, a sensor converging with a source detects a higher frequency than was emitted by the source.

The contribution of the Doppler effect can overwhelm the geometric contributions of special relativistic visualization, rendering the geometry invisible in the resulting image [56].

2.3 Selected Testable Visual Effects

Of the expected Special Relativistic visual effects listed in Section 2.2, the following have been selected as representative and testable with the model developed here. As stated in Section 4.1, it is important to not confuse relativistic effects with classical effects. The relativistic effects to be tested are length-contraction and time-dilation. The classical effects to be tested are retarded time, aberration, and Terrell rotation. These classical effects are also affected by special relativity, which makes them difficult to observe empirically. However, the selected spacetime model will allow the classical and relativistic components of these phenomena to be visualized both separately and together.

2.3.1 Classical Retarded Time

The term ***retarded time*** refers to the delay in the arrival of information about an event due to the distance of an event and the finite speed-of-light. For an observer and an event in the same inertial reference frame, the soonest that the light from an event 10 light-seconds away can reach the observer is 10 seconds after the event has occurred.

As an example, consider the case of a fast high flying jet. The point of origin of the sound seems to trail the jet across the sky due to the finite speed of sound. This effect is merely apparent (a classical effect), not physical (not a relativistic effect). The jet's true position can be measured simply by compensating for the time delay introduced due to the finite speed-of-sound.

Likewise, the appearance of an object is communicated causally to an observer from the spacetime positions of the object at some points in the past. The times that the light left each of the object's surface elements could be different since the object's elements are most likely at different distances from the observer. This will result in a visual distortion of the geometry of the object, if the object is moving with respect to the observer. The greater the velocity, the more apparent the distortion.

The following apparent geometric distortions are visual effects resulting from the aforementioned retarded time phenomena which is an effect of finite lightspeed. The classical effects to be discussed here are non-relativistic aberration, and the non-relativistic component of Terrell rotation. The magnitude of these effects can be affected by Special Relativity.

2.3.2 Classical Aberration

Aberration is a deflection in the distribution of stars in the celestial sphere towards the direction of the motion of the Earth through space. Relativistic aberration is a distortion in the visual sphere about an observer moving through a scene with a relativistic velocity. Non-relativistic or classical aberration is the classical component of aberration that is independent of relativity. As the velocity of the observer increases, the objects in the scene slide towards the front of the observer's sphere of vision. That is, the angle between the observer's velocity vector and the angle of incidence of the light ray from an observed object decreases monotonically as the velocity increases such that the light from the object seems to come from a position closer to the front of the observer. Due to the nature of relativity (the First Postulate), the evaluation gives the same results if the object and observer are exchanged such that the observer is at rest and the object is passing the observer with a relativistic velocity.

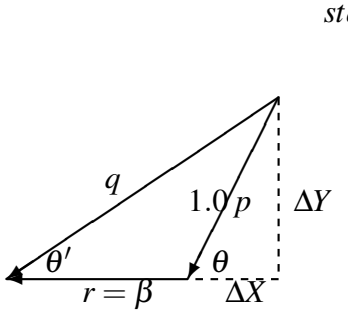

Figure 2.3: Classical Aberration

As shown in Figure 2.3, classical aberration is the apparent angle (θ') of a moving object, which can be determined from simple three-dimensional vector subtraction of the observer's velocity vector (r) from the lightray's velocity vector (p). From the figure, it can be seen that $\tan\theta' = \frac{\Delta Y}{\Delta X + r}$. Scaling the figure so that $p = 1.0$ sets $\Delta Y = \sin\theta$ and $\Delta X = \cos\theta$. This yields the following equation where β is the velocity of the object towards the observer ($\beta = \frac{v}{c}$), θ is the angle of incidence of the lightray to the observer, and θ' is the apparent angle of the lightray to the observer:

$$\tan\theta' = \frac{\sin\theta}{\cos\theta + \beta} \tag{2.1}$$

As can be seen from Equation 2.1, the apparent angle of incidence (θ') of the lightray from the source to the observer will decrease monotonically with respect to the at-rest angle (θ) as the velocity (β) increases.

2.3.3 Relativistic Aberration

Relativistic aberration is the deviation of the apparent angle of a relativistic object from the angle to the object with respect to an observer. This analysis requires the introduction of the Lorentz factor, γ, where $\beta = \frac{v}{c}$:

$$\gamma = \frac{1}{\sqrt{1-\beta^2}} \tag{2.2}$$

The relativistic aberration can be determined from the following equations where α replaces θ as the angle of incidence of the lightray to the observer, and α' replaces θ' as the apparent angle of the lightray to the observer:

$$\cos\alpha' = \frac{\cos\alpha + \beta}{1 + \beta\cos\alpha} \tag{2.3}$$

$$\sin\alpha' = \frac{\sin\alpha}{\gamma(1 + \beta\cos\alpha}) \tag{2.4}$$

$$\tan\alpha' = \frac{\sin\alpha'}{\cos\alpha'} = \frac{1}{\gamma}\frac{\sin\alpha}{(\cos\alpha + \beta)} \tag{2.5}$$

Equation (2.3) was published by Einstein in 1905 [17]. Equation (2.4)'s derivation is shown by Rindler [46]. When Equation (2.5), as shown by Pauli [40], is compared to Equation (2.1), the analytic difference between the classical and relativistic effects can be shown to be a function of Lorentz length contraction:

$$\tan\theta' = \frac{\sin\theta}{\cos\theta + \beta} \tag{2.6}$$

$$\tan\alpha' = \frac{1}{\gamma}\frac{\sin\theta}{\cos\theta + \beta} \tag{2.7}$$

$$\tan\alpha' = \frac{1}{\gamma}\tan\theta' \tag{2.8}$$

A physical interpretation of the Lorentz factor is shown in Figure 2.4 and described as follows. The visual sphere of the observer G in frame *Green*, which G perceives as spherical, appears oblate with respect to the rest frame. The lightray intersects G's visual sphere at angle of incidence, θ where $\tan\theta = \frac{\gamma\,\Delta Y}{\Delta X}$. However, since G sees frame *Green* as at rest and spherical, as depicted by the dashed circle (frame *Red*), G determines the angle of incidence to be $\tan\theta' = \frac{\Delta Y}{\Delta X}$. Consequently, G in frame *Green* perceives the angle of incidence of the lightray to be less than that seen by an observer at rest.

While Equation (2.8) shows an elegant analytical relationship between classical and relativistic aberration, it has a singularity at $\theta = \frac{\pi}{2}$. Terrell [50] solved this problem by using the trigonometric half-angle formula to derive the following relativistic aberration equation:

$$\tan\frac{\alpha'}{2} = \sqrt{\frac{(1-\beta)}{(1+\beta)}}\tan\frac{\alpha}{2} \tag{2.9}$$

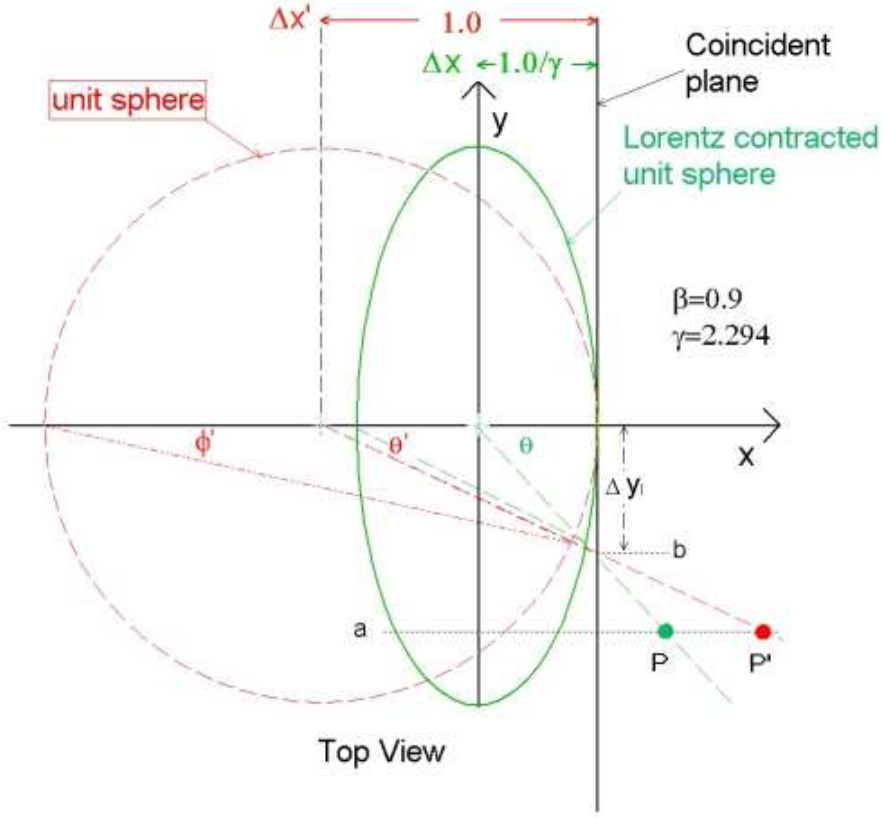

Figure 2.4: Relativistic aberration

As with the classic Equation (2.1) and the relativistic Equation (2.8), the apparent angle of incidence ($\theta'\&\alpha'$) of the lightray from the source to the observer will decrease monotonically with respect to the incoming angle (θ) as the velocity (β) increases. Multiplying Equation (2.9) by $\frac{(1+\beta)}{(1+\beta)}$ yields a more intuitive representation as can be seen from the geometry of Figure 2.4 where the visual sphere is length-contracted by $\frac{1}{\gamma}$:

$$\tan\frac{\alpha'}{2} = \frac{1}{\gamma}\frac{\tan\frac{\alpha}{2}}{(1+\beta)} \tag{2.10}$$

Figure 4.12 clearly demonstrates this relativistic aberration when compared with the classical aberration of Figure 4.11. Figure 4.10 shows the system at rest.

2.3.4 Terrell Rotation

The optical effect known as Terrell rotation can be attributed to a combination of classical effects and relativistic effects: specifically retarded time and relativistic aberration. Since the side facing away from the camera (back) is further from the camera than the side facing the camera, the light from the back will be delayed. Depending on the shape and velocity of the object, it is possible for the object to dodge its own lightray emanating from an obscured

portion of the object. The back or distant portions of an object moving relativistically past an observer, would appear to trail after the object. This effect is clearly demonstrated by the cubes in Figure 2.2 when compared with Figure 2.1, as if they were blowing in the wind. This phenomenon causes the object to appear rotated to face in the direction of its motion, and is known as Terrell rotation.

Although a classical effect, Boas [10] predicted that relativistic straight lines would appear curved to an observer. Terrell [50] predicted that in certain cases the length-contraction could be masked by the classical (Terrell) rotation. Most remarkable is a fast moving sphere. Terrell noted [50] that the Lorentz contraction of an object may be masked by the apparent rotation introduced by the retarded time as described above. In the case of a sphere, the apparent rotation exactly matches the Lorentz contraction such that the silhouette of the contracted and rotated sphere remains a circle. This effect is shown in Figure 2.2

Chapter 3

Spacetime Visualization

3.1 Historical Overview

It is necessary to discuss the history of the visualization of the two fields of relativistically moving objects and multiple dimensions in order to select an optimal strategy to visualize the geometry of spacetime.

3.1.1 Pencil & Paper Analysis

Even before the 20th century, mathematical analysis suggested that objects are *Lorentz-FitzGerald contracted* [11] in the direction of relative motion. This implied that a beach ball moving with sufficient velocity relative to an observer would look like a pancake to that observer, with its symmetrical axis collinear with the velocity vector.

In 1958 Penrose [41], and in 1959 Terrell [50], proved that a relativistically moving object would appear to rotate about the object's axis that is perpendicular to the 1) velocity vector and 2) the line-of-sight vector to the object from the observer in the laboratory (or rest) frame.

Further work was performed by F. Weisskopf in 1960 and Marie Boas in 1961 [10] to prove that the silhouette of a relativistic moving sphere appears to be circular due to the complementary contributions of Terrell rotation and Lorentz contraction.

This seeming contradiction was resolved with visualization software at the end of the 20th century, as shown in figures 2.1 & 2.2 and in the online animations [7]. Note that although the cubes have been distorted, as has the texture map on the sphere in the 86.6%c camera velocity image, the sphere's silhouette is circular as predicted.

3.1.2 Early Four-dimensional Visualization

As early as the 1980's, when commercial workstations were developed with enough power to generate real-time animation, a real-time four-dimensional visualization of a rotating shaded Hypercube appeared as an industry sales demo [6]. Developing Hypercube visualizers has become a popular pastime in the last few years as is evidenced by their proliferation on the Internet [14].

These visualizations treat this hypothetical fourth dimension as simply another space dimension, isotropic and orthogonal to the three space axes. In 1991, Hollasch [24] applied rotations and translations via conventional matrix transforms to project four-dimensional objects onto a three-dimensional hyper-imageplane. This three-dimensional object was then projected onto a two-dimensional screen (or two two-dimensional windows for stereo viewing). In 2001, Mike D'Zmura of UCI created such a virtual four-dimensional world [15] using this isotropic four-dimensional technique that was successfully navigated by test subjects wearing real-time headsets [16].

3.1.3 Relativistic Visualization

Relativistic visualization has been implemented as a four-dimensional application by using the above four-dimensional technologies with a few constraints. Einstein's **SR** and **GR** theories will be addressed separately. The Special Theory of Relativity (**SR**) will be addressed first since it is simpler, requiring simpler algorithms.

Special Relativity: Flat Space Visualization

The most elegant implementation of special relativistic visualization is via four-dimensional object representation, where each vertex of the object is a four component tuple: (t,x,y,z). In addition to the usual three spatial coordinates, there is a fourth t or time coordinate. As with a three-dimensional raytracer, a ray from each screen pixel is intersected, not with a three-dimensional object space, but with the four-dimensional space-time object space. A straight line in four-space will intersect a four-dimensional (flat) space-time (R^4) object in the same way a line in three-space intersects a three-dimensional three-space object (R^3) [34]. If a scalar distance is defined in the usual way, that is as the dot product of a vector with itself, then this dot-product is the solution for the shortest intersection of a light ray from a pixel into the four-dimensional object space. The exact form of the dot product is the ***signature***[1] of the four-dimensional space-time under consideration. In ***Minkowski space*** the lightray's transition time, Δt, is always equal to the path length: $\Delta t = \sqrt{\Delta x^2 + \Delta y^2 + \Delta z^2}$. Therefore, the closest intersection is always the most recent.

In conventional terms, each vertex of the object is represented as a four component coordinate or four-tuple as in (t,x,y,z). Where the t component represents the particular vertex's location at time t. Thus a stationary sphere would trace out a hyper-cylinder along the t axis in this four-space, analogous to a circle extruded into a cylinder in a (2+1)D spacetime. A moving sphere of constant velocity would trace out a hyper-cylinder at an angle to the negative t axis. This angle would be larger if the object's velocity were larger.

[1] The ***signature*** of a spacetime, also referred to as its ***metric***, is the coefficient matrix used to generate the dot-product for distance calculation. The Minkowski metric yields a distance function where Δs is the distance between two events and is given by: $\Delta s^2 = (-1)\Delta t^2 + (+1)\Delta x^2 + (+1)\Delta y^2 + (+1)\Delta z^2$. $(-1,+1,+1,+1)$ is the signature of Minkowski spacetime.

General Relativity: Curved Space Visualization

A difference between Special Relativity and General Relativity is that in the latter the space is not only warped, but it warps dynamically. The local warp is a function of the local energy. This warp bends the light rays, and the light rays (mass or energy) cause the warp. Consequently, intersection of a light ray and a four-dimensional object is no longer a case of intersecting a straight line with an object in a four-dimensional object-space-time. The light ray in GR must be modeled by a non-linear curve [5]. The light ray can bend, as is evidenced by 'gravity-lensing'.

3.1.4 Multidimensional Models

String theorists cavalierly refer to 10, 11 and 26 dimensional universes. Large Extra Dimension (*LXD*) models are appearing in contemporary physics literature [4][44]. Exploring higher dimensional representations of empirical physical phenomena may yet lead to a new and profound understanding of the nature of our Universe beyond the *Standard Model*[2] of three spatial dimensions or four spacetime dimensions. Nordstrom [37], Kaluza [31], and Klein [32] introduced theories that include five spacetime dimensions. Visualization of these five-dimensional models is a challenge that has yet to be explored.

3.1.5 Spacetime Visualization

Spacetime visualization is a new field that needs to be adequately addressed in its own right. Spacetime visualization can be considered as Euclidean four-dimensional visualization with constraints. These constraints are: 1) a constant finite limit on lightspeed; 2) each inertial reference frame has its own orthogonal time axis collinear with its instantaneous velocity 4-vector; and 3) the Lorentz group [3] describes the transform between time-axes and their associated frames.

3.2 Related Technologies

Various algorithms and techniques have been developed by physicists, scientists and educators for visualizing relativistic effects in Minkowski four-dimensional spacetime [23, 25, 49, 55]. Conventional three-dimensional visualization techniques have been adapted to relativistic visualization applications. These techniques include polygon rendering, ray tracing, radiosity, texture-based rendering and image-based rendering. A short discussion and examples are provided for each technique. An in depth description of each of these techniques can be found in *Visualization of Four Dimensional Spacetimes* [56].

[2]The standard model is the current theory of fundamental known particles and how they interact. This successful theory includes the strong and electroweak forces, but not gravity. [33]

3.2.1 Special Relativistic Polygon Rendering

In Euclidean four-space, the polygon rendering approach is implemented by extending the algorithms of three-dimensional object projection to four-dimensional objects in order to project these four-dimensional objects onto a conventional two-dimensional imageplane [13]. Since special relativistic visualization occurs properly within the context of a non-Euclidean four-dimensional spacetime, the approach for visualizing four-dimensional spacetime is subtly different from that for a Euclidean four-space. While not necessary for the Euclidean four-space approach, a Lorentz transform[3] is necessary in the non-Euclidean four-space to convert from the object's inertial reference frame to the inertial reference frame that contains the imageplane (the camera frame).

Hsiung and Dunn [25] used image shading of fast moving objects in 1989. Hsiung, Thibadeau, and Wu [30] implemented an optimized strategy in 1990 with their novel time-buffer approach, which used graphic Z-Buffer hardware to optimize performance. The time-buffer algorithm performed conventional three-dimensional rendering in the object's rest frame, and then performed a Lorentz transform operation on each of the lightrays in the object's imageplane to convert to the camera's imageplane. The time-buffer then filtered for the most recent ray-object intersection event for each pixel.

Rau, Weiskopf, and Ruder [45] implemented a polygon renderer in 1997 in which the three-dimensional objects in the object frame were Lorentz transformed into three-dimensional *photosurface* objects in the camera frame. The new *photosurface* object, which approximated the shape of the object as viewed from the camera frame, was then projected onto the camera's viewplane using conventional three-dimensional rendering techniques.

Resulting color and brightness can be found by applying analytic Doppler and searchlight models to the object's color [28].

Traditional rendering techniques are applied to render a series of still frames. Moving objects with identical velocities (including the camera or observer) are grouped into *inertial reference frames*. Conventional R^3 transforms are applied to the frames. "Photo-surfaces" are then produced. Shadowing and conventional lighting models are selected and then applied to the photo-surfaces. Lorentz contraction is applied to the geometry of all the objects (polygons via their vertices) in each of the frames. Accelerated observers and objects can also be handled via the technique of ***Momentary Comoving Reference Frames*** (***MCRF***). Shadowing and moving light sources can be similarly handled.

This technique must be considered a model of a model - i.e. the visualization models the mathematical model of the physical event. The technique improves performance by taking advantage of customer-off-the-shelf (COTS) video game hardware. However, assumptions are made about the physical phenomena in order to exploit optimization. These assumptions, while providing reasonable mathematical approximations, may be physically invalid. Optimization and any assumption are problematical at this stage of research since there is no empirical data with which to compare the visualization's results.

[3] "the Lorentz transform corresponds to a 'rotation' of the co-ordinate system in the four-dimensional 'world"' - Einstein [20].

3.2.2 Special Relativistic Ray Tracing

In 1988 Glassner [23] developed an optimization strategy exploiting temporal coherence for conventional three-dimensional raytracing. In his approach, three-dimensional objects were raytraced in four-dimensional space, resulting in up to 50% processing time improvement. He also demonstrated that motion blur could be generated by varying the camera's time component. Although he did not demonstrate relativistic visualization with his algorithm, he did suggest it as a direction for future research.

Hsiung and Dunn [29] suggested a three-dimensional raytracing static solution to display the apparent geometry of a relativistic object, and also the inclusion of a spacetime model [26]. In their implementation, three-dimensional objects were imported and maintained in their own inertial reference frame in which they are at rest.

First, a lightray is projected back in time from each screen pixel, in sequence. The camera parameters provide the starting three-dimensional point and direction vector for the ray.

Second, for each Inertial Reference Frame, the ray is transformed from the camera frame (S_{cam}) into the object's frame (S_{obj}) via a *Lorentz Transform* (which changes the angle of the lightray with respect to the reference frame), and intersected with the three-dimensional object in the object's rest-frame. The event closest to S_{cam} (most recent) is selected for determining the appropriate pixel color.

Third, conventional three-dimensional raytracing lighting models can be implemented along with the addition of the Doppler and searchlight effects. In all cases, the object contains lighting model parameters (color, reflectivity, etc.). A technique for color power spectrum processing via B-spline interpolation was implemented by Hsiung, et. al. in 1990 [27].

Fourth, as with three-dimensional raytracing, lighting is calculated recursively to a specified depth. The deeper the recursion, the more photo-realistic the image. Each reflected (or refracted) lightray is recursively *Lorentz-transformed* from S_{obj}'s rest frame into the reference frame of subsequent S_{obj}'s as with the Second step, above.

In 2001, a promising approach was introduced by Weiskopf in his PhD Dissertation [56] in which he described and built a four dimensional General Relativity ray tracer. This model supported only geometric effects, and secondary rays and shadow rays were neglected.

3.2.3 Special Relativistic Radiosity

Radiosity [12] is based on global energy conservation, and works well for diffuse shadowing. Radiosity first determines the radiant energy at surface patches independent of the viewer's position. A renderer then computes the view from a particular position. Daniel Weiskopf, et al [53], developed a relativistic extension of radiosity that allows rendering of diffusely reflecting scenes.

The technique is good for relativistic fly-thru's of static scenes, since the rendering phase can be performed by conventional graphics hardware. However, the researcher is limited to stationary scenes.

3.2.4 Special Relativistic Texture-Based Rendering

The Special Relativistic Texture-Based rendering strategy uses contemporary graphics hardware to render relativistic geometry and illumination in realtime. Weiskopf developed an OpenGL implementation and demonstration of this technique [56].

Techniques were proposed in 1999 and 2000 to use texture mapping hardware to view apparent geometry [51] and relativistic illumination [52]. This technique simulates searchlight, aberration, and Doppler effects, which can be combined in a plenoptic function. The technique allows interactive frame rates by judicious use of contemporary graphics texture mapping hardware. However, the researcher is limited to these predefined searchlight, aberration, and Doppler models.

3.2.5 Special Relativistic Imagebased Rendering

Imagebased relativistic rendering utilizes the techniques developed for three-dimensional imagebased rendering [39], and has all the advantages of imagebased rendering: no three-dimensional modeling, rendering is quick, photo-realism is easy. Movies based on videos recorded by off-the-shelf cameras at non-relativistic velocities can thus easily produce realistic appearing relativistic images. A major limitation here is that the sampled image does not allow for relative motion of the objects. Only the camera (S_{cam}) can move relativistically.

The strategy was implemented by applying relativistic aberration to each pixel of the visual sphere surrounding the observer, thus warping the geometry of observed objects. If a wavelength-dependent plenoptic function is provided with sufficient bandwidth, then the transformed pixel's power-spectrum can be generated from the untransformed image. [54] The algorithm can be adapted to texture mapping hardware for real-time performance with data acquired by standard cameras.

3.3 Proposed Strategy

Elegance is the goal with any software strategy. An algorithm with no special cases is optimum: an algorithmic strategy, a model, from which the empirical evidence will naturally and transparently emerge. Optimization strategies may encompass shortcuts and assumptions, but the research model must not be so compromised. Of the above described strategies, special relativistic raytracing in four-dimensions provides the simplest model of the observed behavior of light, and holds the greatest promise.

3.3.1 Special Relativistic Four-dimensional Raytracing

Since space is 'flat' in Special Relativity, a lightray is a straight line in four-space, just as it is in three-space. A four-dimensional lightray can thus be intersected with the four-dimensional objects in four-dimensional space just as a three-dimensional line can be with objects in three-dimensional space. So the heretofore three-dimensional coordinates (x,y,z)

of each object are maintained as four-dimensional coordinates (t,x,y,z). The procedure was to implemented as follows.

First, a four-dimensional straight lightray is projected back in time from each screen pixel, in sequence. The camera parameters provide the starting four-dimensional point and four-dimensional direction vector for the ray. However, since the fourth-dimensional axis in this implementation is the time axis, certain constraints are made upon the ray in four-dimensions. Specifically, the ray must maintain a 45 degree angle with the negative time axis. Other constraints will be discussed in Section 4.3.2.

Second, this four-dimensional ray is intersected with each object in the four-dimensional database, as is the three-dimensional ray in conventional raytracing. The intersection algorithm is described in Section 4.3.

Third, for each intersection, the ray is transformed from the camera frame (S_{cam}) into the object's frame (S_{obj}) via a Lorentz Transform derived from the information in the object's ***inertial reference frame*** (**IRF**). Each intersection corresponds to a possible emission, reflection, or refraction event. The event closest to S_{cam} (most recent) is selected as the appropriate intersection event.

Fourth, the selected lighting model, such as the Hsiung model [28] wherein the spectral power distribution is carried along with the lightray, is implemented in S_{obj}. The object contains lighting model parameters (power-spectrum or color, reflectivity, etc.).

Fifth, as with three-dimensional raytracing, lighting is calculated recursively to a specified depth. The deeper the recursion, the more photo-realistic the image. Each reflected (or refracted) lightray is recursively transformed from S_{obj}'s rest frame into the reference frame of subsequent S_{obj}'s as with the Third step, above.

This technique appears to be the 'best of breed'. The implementation is most realistic, in the sense that it implements a simple and honest simulation of first principles, and hence could lead to the discovery of new principles of physics.

Subsequent modifications have been made to this procedure. Specifically, an arbitrary laboratory inertial reference frame has been established wherein the camera may be considered to be at rest. The relativistically moving objects were Lorentz transformed from their rest frame into this laboratory frame. Essentially their four-dimensional geometry was modified prior to insertion into the database - the objects were length-contracted and time-dilated. The object's surface color parameters could also be modified to represent their state as transformed into S_{cam}. This preprocessing step simplified run-time steps three and four, so that conventional three-dimensional raytracing techniques could be applied as described in Section 4.3.

Chapter 4

Implementation

The challenge is to go beyond visualization of special relativity or spacetime. This thesis provides a method for visually conceptualizing higher dimensions. The strategy is demonstrated using four-dimensional spacetime (3 spatial + 1 temporal dimensions), a dimensionality that has been visited in the computer graphics literature. Since it is possible to conceptualize spacetime viewing by extrapolating from three-dimensional viewing, it may also be possible to view higher dimensions by a similar process.

In the selected approach, time is treated as a fourth geometric dimension with certain constraints described below. The results of viewing this higher dimensional spacetime are compared to the results of contemporary special relativistic visualization. If this strategy yields similar results, it should be possible to create a simple yet accurate model for a geometric interpretation of Einstein's spacetime and a pedagogy to explain the phenomena. For simplicity, it is assumed that spacetime is flat, there is no acceleration, and the camera is at rest in the laboratory's inertial reference frame (the camera frame). The single light source is also at rest in the camera frame.

The selected geometric model treats three-dimensional objects as cross-sections of four-dimensional objects projected into three-space. The four-space is probed via photon paths which lie on the surface of a right circular hypercone, known as the ***lightcone***. The lightcone's symmetrical axis is collinear with the negative time ($-t$) axis. This results in a cross section of four-space that corresponds to the intersection of the lightcone's surface with embedded 3-manifolds. The resulting visualization of this projection should have the same properties as those provided by contemporary relativistic visualization tools.

The 3+1 dimensional approach was selected to adhere to Einstein's geometric vision of light propagation [18]. Representing three-dimensional objects in spacetime and ray tracing three-dimensional manifolds in four-dimensional is explained in detail beginning with a brief overview of the theory, then presenting the simple geometric algorithms and their implementation.

4.1 Task Definition

This chapter will visually explore two phenomena of spacetime: the visual effects of finite lightspeed; and the physical effects of Special Relativity. The former visual effects[1] which

are due to the ***retarded*** (delayed) light signal will be referred to as ***classical***, while the latter effects will be referred to as ***relativistic***. There is an interesting relationship between the ***classical*** and ***relativistic*** phenomena as pointed out by Terrell [50], Penrose [41], and Boas [10]: in that the two effects can cancel each other out in some cases.

The *classical* effects of finite lightspeed are simply the apparent distortions to an object that are the result of light from portions of the object at different distances from the observer arriving at different times. A rapidly moving object's physical shape can be determined simply by compensating for the delay introduced by the finite speed of light. *Relativistic* effects result from special relativity, and are real and physical, not merely apparent.

The following sections will graphically demonstrate that a geometric model can be created wherein three-dimensional objects are considered to be cross sections of four-dimensional objects projected into three-space, and that the four-dimensional objects can be treated as rigid, assuming that there is negligible mass. A method is provided to convert a given three-dimensional object into a four-dimensional spacetime object, and to observe the converted objects from the camera's inertial reference frame. This geometric implementation will be shown to yield results equivalent to those of prior non-geometric less simple visualizations.

4.2 A New Approach

The techniques designed to visualize special relativity typically use three-dimensional ray-tracing of three-dimensional objects, with additional logic to handle the velocity matching and Lorentz transforms, operations that are not required with three-dimensional visualization. It would be advantageous if an algorithm could be found for which no special logic and transforms are required to simulate the geometry of relativistically moving objects. A suitable algorithm would reduce the special cases and associated logic to less than that required with three-dimensional visualization.

Traditional three-dimensional animation simulates the motion of objects by repositioning the objects in the scene between frames. In the method described here, the four-dimensional objects are static, and only the camera's temporal position is changed between frames. The novelty of this model is its adherence to a geometric interpretation of Einstein's spacetime concepts[2]. The postulates and fundamental principles of relativity are used as the basis for these techniques. Ray tracing of four-dimensional spacetime was selected as the best technology due to its conformity to a more natural interpretation of Einstein's spacetime. This model also introduces ***temporal extrusion***, a simple operation to extend a three-dimensional object into four-dimensional spacetime. For simplicity, this thesis will emphasize the visualization of the geometry of objects with constant velocities. Although not demonstrated here, the concepts can be generalized to accelerating objects with curved four-dimensional paths via curved temporal extrusions.

[1] Sometimes referred to as Newtonian relativity. The Galilean transform assumes that the geometry of space is Euclidean.

[2] "... the four-dimensional space-time continuum of the theory of relativity, in its most essential formal properties, shows a pronounced relationship to the three-dimensional continuum of Euclidean geometrical space." - Einstein [21]

4.3 The Algorithm

In order to visualize both the classical and relativistic effects described in Section 2.3.4, a modified raytracing mechanism was chosen to represent the geometric model described by Einstein[3]. The presented variant of raytracing, unlike conventional raytracing implementations, takes into account the finite speed of light.

A conventional raytracing engine determines the color of a pixel by passing a lightray from the camera through each pixel of the image plane and out into the three-dimensional scene. If the lightray intersects an object, then the color of the object, modified by a suitable color model, is transferred to the pixel of the image plane. The algorithm is more complex when the lightray has a finite velocity.

In order to find the intersection of a finite speed lightray with three-dimensional objects, the model must account for the changing positions of moving three-dimensional objects as the lightray travels towards the camera. For multiple intersections the model must find the object-intersection closest to the camera. Furthermore, the model must account for length-contraction and time-dilation.

From the Principles of Special Relativity as delineated in Sections 4.1 and 2.1, the following set of specifications was formalized.

1. All objects in the scene will be instantiated in a common laboratory inertial reference frame. The camera and light source, both at rest, will be instantiated in the laboratory frame.

2. A four-dimensional object is created from a three-dimensional object by ***temporal extrusion***, that is extruding the object along its velocity 4-vector in the laboratory frame:
   (a) The velocity of the extruded object is the extrusion's spatial change divided by the temporal change;
   (b) If an object's extrusion vector (worldline) is parallel to the camera's t axis, then the object appears to be static; otherwise it appears to be moving;
   (c) The Lorentz transform (LT) is determined from the object's extrusion vector's spatial to temporal ratio ($\frac{\Delta x}{\Delta t}$) as follows:
      i. $\beta = \frac{\Delta x}{\Delta ct} = \frac{\Delta x}{\Delta t} \times \frac{1}{c}$
      ii. $\theta = \operatorname{arctanh} \beta$
      iii. $$LT = \begin{pmatrix} \cosh\theta & -\sinh\theta & 0 & 0 \\ -\sinh\theta & \cosh\theta & 0 & 0 \\ 0 & 0 & 1 & 0 \\ 0 & 0 & 0 & 1 \end{pmatrix}$$
   (d) The Lorentz transform is applied to the object prior to the object's insinuation into the laboratory frame (except *Lorentz-decoupled* objects). Length-contraction modifies the object geometry, and time-dilation modifies time dependent aspects of the object such as its color and lifetime.

[3] "Formally, these four co-ordinates correspond exactly to the three space co-ordinates in Euclidean geometry" - Einstein [21]

3. Lightrays will be constrained to lie on the hypersurface of a right circular hypercone symmetric about the t axis thus yielding a constant lightspeed ($c = 1.0$) in natural units. This hypersurface bisects the angle between the negative time axis and the spatial axes.
4. For each video-frame, an image will be generated by iteratively passing a ray from the camera's POV through each pixel in the imageplane (or visual sphere about the POV) such that the ray lies on the hyperconical surface, and out into four-space where it may intersect with a 3-manifold defining a four-dimensional object in the four-space. For multiple intersections, the intersection closest to the camera (most recent) is selected.
5. For each video-frame, imageplane pixels will be colored by extracting the three-dimensional properties of the Lorentz transformed four-dimensional object at the point of lightray/object intersection. It shall be assumed that the light source is at rest in the laboratory (camera) frame, and that the contributions of the moving objects to one another's local diffuse lighting are trivial (and does not contribute to the objects' geometry).
6. Advancing the camera along the t axis is equivalent to advancing the scene ahead in time. A sequence of animated views will be generated by incrementing only the t component of the camera's (and viewplane's) four-dimensional position for each video-frame with no modification to the objects in the worldspace.

4.3.1 Object Construction

A three-dimensional object can be visualized by rendering the two-dimensional faces connecting its one-dimensional edges. The four-dimensional objects shown here are visualized by rendering the three-dimensional hyper-faces connecting their two-dimensional faces (Figure 4.1).

Extrusion is a common three-dimensional Computer Aided Design (CAD) operation whereby a two-dimensional object is transformed into a three-dimensional object by extruding the object along a vector perpendicular to the plane in which the two-dimensional object lies. Likewise, the extrusion of a three-dimensional object into four-space is accomplished by extruding the object along a vector perpendicular to the hyperplane (three-space) in which the object lies.

Temporal extrusion is a similar spacetime operation. A three-dimensional object is extruded along a vector perpendicular to the hyperplane in which the object lies. That perpendicular is the *object*'s proper time axis (*not* the camera's time axis). Since the object's velocity vector is also the object's time axis in this model, the object is actually extruded along the velocity 4-vector.

As with conventional three-dimensional rendering, complex objects are constructed from simple primitives. In this case, the primitives are two-dimensional triangles in three-dimensional space extruded along their common time axis into four-dimensional. For example, each of the 12 triangles of the cube in Figure 4.1a is extruded parallel to its time axis for a distance equivalent to the time the cube is in existence (and at a constant velocity) thus creating a three-dimensional hypersurface (or 3-manifold) in four-space (Figure 4.1b).

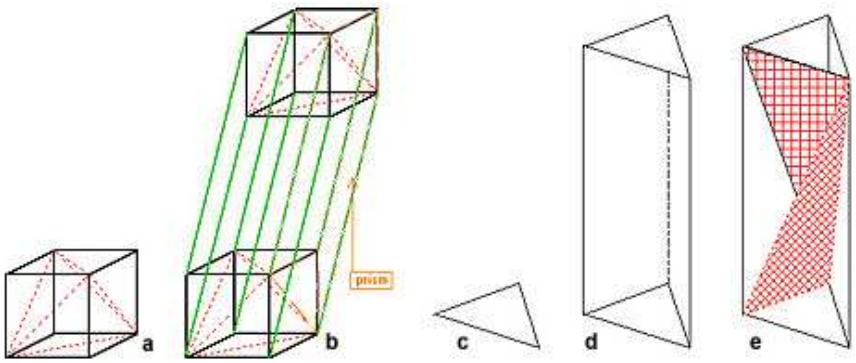

Figure 4.1: Cube & Triangle: Extruded then tessellated

Any three-dimensional object defined by bounding triangles (Figure 4.1) can be ***temporally extruded*** into a four-dimensional hyperobject and inserted in the scene's four-space (the model database) as follows. First insert a t component into each of the vertex coordinates and set t to some constant value, say t_0:

$$(x_i, y_i, z_i) \rightarrow (t_0, x_i, y_i, z_i).$$

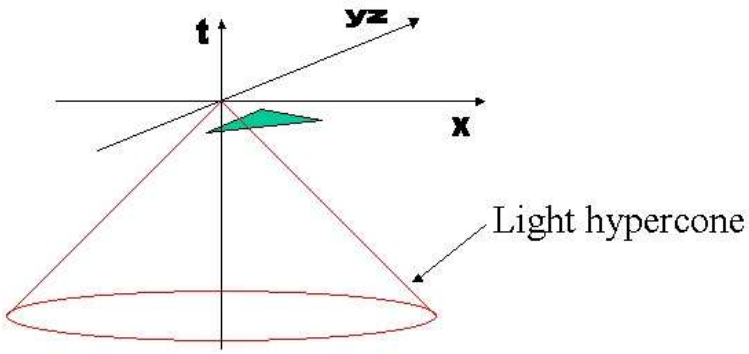

Figure 4.2: 2D face prior to temporal extrusion

The object now lies embedded in the t_0 hyperplane orthogonal to the t axis (Figure 4.2). In other words, the object instantly appears for a moment at $t = t_0$. Each of these triangles, and hence the object composed from them, can be extruded into the 4th dimension by duplicating the vertices of the triangle with lessor (or greater) values for the t components. If the object is at rest in the camera frame, a constant, Δt, can be added to the t components, before each triangle is extruded from the original (t_0) hypersurface to the new duplicate ($t_0 + \Delta t$) hypersurface. As in Figure 4.3 where $\Delta t < 0$, connecting the respective vertices of the extruded and original triangle pairs creates a prism from each triangle:

$$(x_i, y_i, z_i) \rightarrow (t_0, x_i, y_i, z_i) + (\Delta t, \Delta x_i, \Delta y_i, \Delta z_i) \rightarrow (t_1, x_i, y_i, z_i)$$
$$\textit{where} \;\; \Delta x_i = \Delta y_i = \Delta z_i = 0 \rightarrow v = 0$$

The prisms are then tessellated into three adjacent tetrahedra simply by using a table to connect two triads of vertices by way of two triangles as shown in Figure 4.1. The

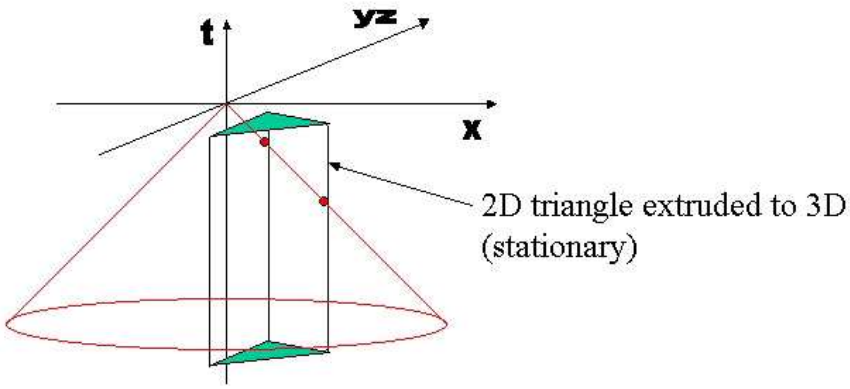

Figure 4.3: Triangle at rest extruded through lightcone

three-dimensional simplices are necessary for the Barycentric algorithm used to find precisely where, *on* the 3-manifold (i.e. *within* the three-dimensional hyper-face) of the four-dimensional object the intersection with the ray occurs.

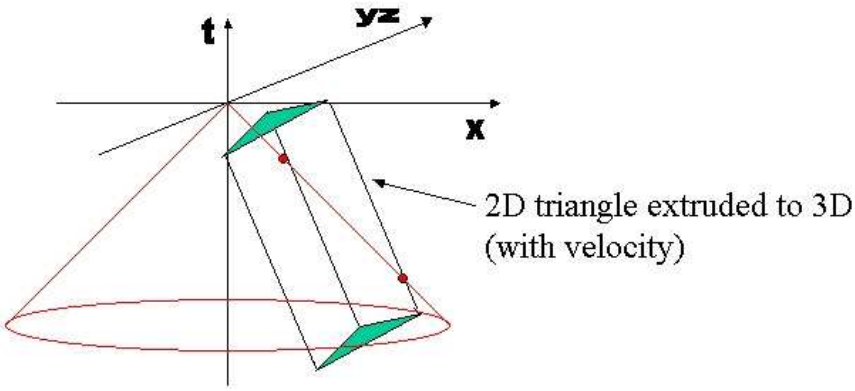

Figure 4.4: Temporal extrusion not parallel to 't' axis

An object's velocity is represented by changing the position of the extruded end of the triangle (Figure 4.4) with respect to the original end, e.g. $x_{end} = x_{beg} + 2.0$, so that $\Delta x = 2.0$ spatial units. The speed would thus be $2.0 \frac{spatial\ units}{time\ unit}$.

Two classes of three-dimensional objects have been implemented in the software: the Hyper-object (H_{obj}) and the Virtual-object (V_{obj}). Conceptually, the H_{obj} is observed passing through the laboratory inertial reference frame at a relativistic velocity, and so the measurements of the object are already in the laboratory's subjective units, meaning it is already length-contracted and time-dilated. This H_{obj} is added to the database using its subjective dimensions as seen in the camera frame, since it is already Lorentz transformed. This H_{obj} class is used to specify *Lorentz-decoupled* objects.

The V_{obj} is likewise passing through the lab frame at a relativistic velocity, but has been observed at rest, and the object size is obtained from its own rest frame. The V_{obj} is entered into the database using its proper rest dimensions, and a velocity vector in the laboratory (camera) frame. The virtual object must thus be Lorentz transformed from its rest frame to

the laboratory frame as it is instantiated in the scene. The velocity 4-vector $(\Delta t, \Delta x, \Delta y, \Delta z)$ contains the numeric lifetime of the object as the temporal (Δt) component, and the travel distance in time Δt as the spatial $(\Delta x, \Delta y, \Delta z)$ components.

If an object's extrusion vector is kept to less than 45° with respect to the t axis (i.e. inside the lightcone), then it will have a velocity less than that of light. As an interesting aside and an extension to the standard model, super-luminal velocities may be represented via (Lorentz-decoupled) objects with extrusion angles greater than 45°.

4.3.2 Viewing Three-dimensional Objects in (3+1)D Spacetime

Consider a three-dimensional viewfrustum in three-space (x, y, z), whose camera lies at the origin, and whose line-of-sight is collinear with the x axis. If a three-dimensional object such as a cube were placed within the three-space viewfrustum, the object can be viewed via traditional raytracing.

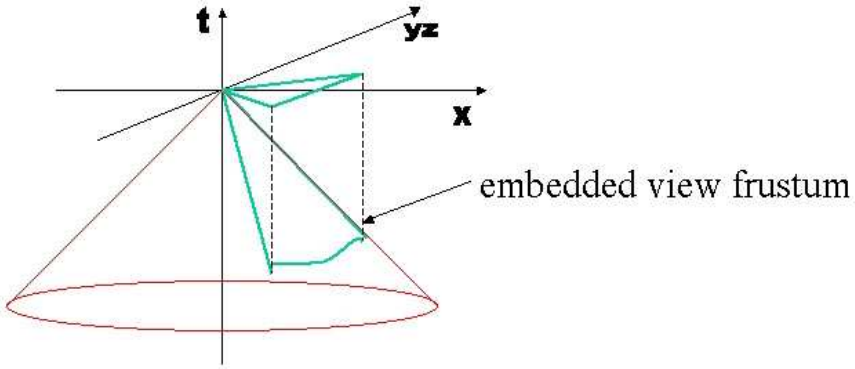

Figure 4.5: Viewfrustum projected onto lightcone

Figure 4.5 depicts a hypercone in four-space (t, x, y, z), whose symmetric axis is collinear with the $-t$ axis, and whose apex is coincident with the origin $(0, 0, 0, 0)$. This hypercone's hypersurface has 3 dimensions, sufficient to contain the three-dimensional viewfrustum. Although it is a 3-manifold in four-space, this hypercone is known as a ***lightcone***.

Conceptually, to account for the finite speed of light, the viewplane can be considered to be spherical thus allowing lightrays from all pixels to reach the view point at the same time, so that the viewfrustum light delay does not contribute any geometric distortion. This viewplane is extruded along the negative time axis and is guaranteed to remain on the light cone. Such an extrusion is shown in Figure 4.5. Since it is a right circular hypercone, the four-dimensional camera coordinate is $(0,\ 0,\ 0,\ 0)$, while the viewplane coordinates for each pixel (p) are

$$(t_p, x_p, y_p, z_p) = (-\sqrt{x_p^2 + y_p^2 + z_p^2}, x_p, y_p, z_p) \tag{4.1}$$

As depicted by the red or shaded dots in Figures 4.3 & 4.4, a camera located at the origin of this four-dimensional model can see only those three-dimensional objects whose extruded tetrahedra intersect the lightcone, that is vertex extrusion pairs (t_0, x_i, y_i, z_i) & (t_1, x_i, y_i, z_i), where

$$t_0 \geq \sqrt{x_i^2 + y_i^2 + z_i^2} \geq t_1, \forall \ \{(t_0, x_i, y_i, z_i) \ \ \& \ \ (t_1, x_i, y_i, z_i)\} \tag{4.2}$$

Lightcone crossing events are detected by solving for the intersection of a lightray with each of the bounding tetrahedra. The set of lightrays is defined as that set of four-dimensional straight lines passing from the camera through each of the pixels in the viewplane's pixel grid and out into four-dimensional space. Using a barycentric algorithm the intersections of the ray with all tetrahedra faces are determined, and that intersecting event nearest to the camera (i.e the t value closest to 0.0) is selected. The array of one-dimensional lightrays that originate from the gridded viewplane results in a two-dimensional image of the object(s) projected onto that viewplane.

Since the objects have been Lorentz transformed prior to the intersection, such that their geometry is correct for the camera frame in which the intersection occurs, the geometric components of the lighting model, the surface normal and the reflection angle, can be used to determine that pixel shade just as with a conventional lighting model in three-dimensional rendering.

If the true pixel color is required, a relativistic Doppler shift must be applied to the color model at the surface intersection. This later step is not necessary to view the geometry of the object(s), and may in fact hinder the object's visibility since, at relativistic velocities, light can Doppler shift out of the visible range.

4.4 Results

It is critical that both the physical model as well as the visual representation are accurate and properly resolve relativistic optical properties. That is, if the four-dimensional spacetime model is accurate, then it can be expected to manifest certain relativistic optical properties. Among these are motion, retarded time, Terrell rotation and relativistic aberration. Two characteristic classes of optical phenomena were examined and compared: low-speed effects and relativistic effects.

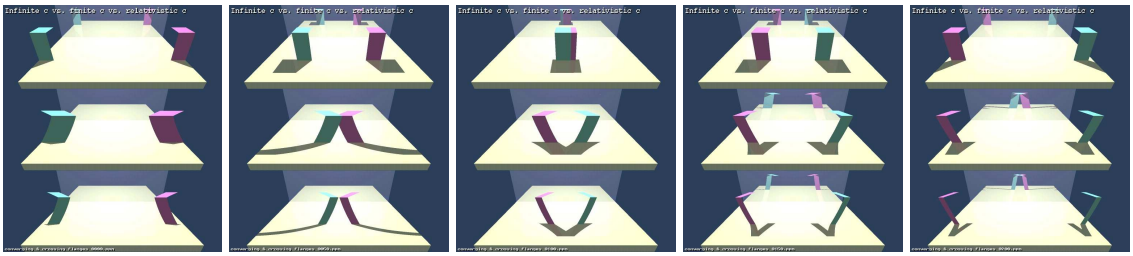

Figure 4.6: 4D objects converging then crossing at 0.866 c on a mirrored background

Low-speed effects are, in this case, those for which the magnitude of the velocity vector of the object frame is less than 1% of the speed of light with respect to the camera frame: typically much less than 3,000 km/sec. Those speeds encountered in day-to-day activities are in this category. For convenience, a relativistic velocity of 0.866c was used to visualize the relativistic effects, since at 86.6% of lightspeed the Lorentz factor is 2.0: objects contract to $\frac{1}{2}$ their rest length; and the object's time dilates to twice its proper time. In other

words, the object's meter sticks are $\frac{1}{2}$ of a meter long as measured in the rest frame; and for each second that is ticked off by the object's clock, two seconds will pass in the rest frame.

The non-relativistic objects in this model travel at $0.00866c$. In some cases, an instantaneous lightray was used (i.e. the lightspeed was set to infinity) to show by comparison, the effects of a finite lightspeed.

A *Visual Software Test Fixture* (VSTF) was created that would display animated sequences for user specifiable object shapes, positions and relativistic velocities, as well as camera position, attitude and velocity. The VSTF displays both three-dimensional and four-dimensional objects allowing visualized four-dimensional objects to be compared to three-dimensional test points visualized via conventional algorithms. The VSTF can operate in a debug mode, providing a means to interactively examine variables or to log results for later comparison against expected results.

For the following test cases, the unit of time is the tick of an arbitrary clock, and its spatial unit is the distance that light travels in one tick of this universal clock. As stated in Section 2.1, natural units will be used throughout such that the unit of measure for the spatial axes and the time axis is the generic *unit*. However, for pedagogical clarity the time (t) axis units will be referred to by the term $t.unit$s and the spatial units will be referred to as $l.unit$s, but $t.unit \equiv l.unit$.

As shown in Figure 4.7, the VSTF displays a stage overlaid with a 12x12 grid. The red (darker shaded) grid lines with cross-section of $\frac{1}{20}$ of an $l.unit$, are on one $l.unit$ centers, as are the red (or darker shaded) rungs on the green (or lighter shaded) rails suspended four $l.unit$s above the stage. The green (or lighter shaded) grid lines represent the X and Z axes on the stage. The stage and these tick-marks as shown are identical for both non-relativistic and relativistic images. Light takes about 8.66 seconds to cross the stage. To give a sense of scale, this is equivalent to a 2.596 million km stage which could comfortably accommodate Jupiter and the orbit of its moon, Ganymede. Each $l.unit$ is 216,350 km, and a $t.unit$ is 0.721 seconds. The corresponding animations were rendered at 10 video-frames per $t.unit$ (except for the example in section 4.4.2) and are available online at [8].

Figures 4.6 - 4.15 demonstrate that the spacetime model accurately displays a three-dimensional object moving at up to relativistic velocities and accurately renders the effects of retarded time, Terrell rotation, and aberration. The two figures, 4.7 & 4.8, demonstrate that for non-relativistic motion (e.g. $\beta = 0.00866$), the model yields the expected results.

4.4.1 Animation as a Property of Spacetime

Although not an emergent property[4], animation of a three-dimensional object *emerges* as a result of the object's representation within this four-dimensional spacetime model. Video-frames from the animation are shown in figures 4.7 and 4.8. These images were rendered by moving the camera from $(t,x,y,z)_{cam} = (940,0,6,15)$ for video-frame 920 to $(t,x,y,z)_{cam} = (1171,0,6,15)$ for video-frame 1151 (the camera was moved ahead 20 frames to allow enough time for the light to reach the camera). The accompanying animation sequences further demonstrate the emergence of animation from a *static* spacetime

scene.

In these sequences, the simple right-angle flange has the following dimensions: 4.0 *l.unit*s high by 2.0 *l.unit*s wide by 2.0 *l.unit*s deep. The faces have no depth (being merely two-sided planes). The flange is constructed and temporally extruded as described in Section 4.3.1

4.4.2 Retarded Time

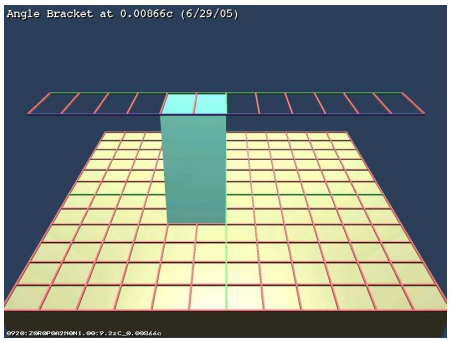

Figure 4.7: Right moving flange at $x = 0$ in video-frame 920.

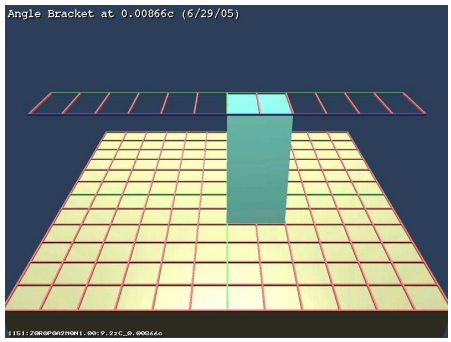

Figure 4.8: Right moving flange at $x = 2$ in video-frame 1151.

In the first demonstration, the flange was encoded with an angle corresponding to a velocity of $0.00866c$, by offsetting the flange during the extrusion process as described in Section 4.3.1. A Δx of 17.32 *l.unit*s for an elapsed time (Δt) of 2000 *t.unit*s was coded, yielding

$$V_{exp} = \frac{\Delta x}{\Delta t} = \frac{17.32\ l.units}{2000\ t.units} = 0.00866 \frac{l.units}{t.unit} \tag{4.3}$$

In Figure 4.7, the flange is moving from left to right at 0.866% of lightspeed. Using the crossing green lines on the stage as the origin, the camera is at $(0, 9, 15)$. Figure 4.7 shows the position of the moving flange with respect to the stage's grid marks within 0.05 *l.unit*s. Note that the flange lies exactly between $x = -2$ and $x = 0$.

Examining Figure 4.7 and Figure 4.8 demonstrate that the algorithm is accurate. Figure 4.7 shows video-frame 920 with the right edge of the flange at the center gridline $x = 0$ of the stage. Figure 4.8 shows fame 1151 with the right edge of the flange at $x = 2$, giving a Δx of 2.0 ± 0.05 and a Δt of 231. At an animation rate of 1 *t.unit* per video-frame, this yields a velocity of approximately

$$V_{obs} = \frac{\Delta x}{\Delta t} = \frac{2}{231 * 1} \frac{l.units}{t.unit} = 0.00866 \frac{l.units}{t.unit} \pm 2.5\% \tag{4.4}$$

By comparing Figure 4.7 at video-frame 920 with Figure 4.8 at vide-frame 1151 it can be seen that the image of the flange has moved 2.0 *l.unit*s in 231 video-frames (231 *t.unit*s) or 0.008658 $\frac{l.units}{t.unit}$, within the expected value to better than 0.02% at non-relativistic speeds. The accuracy thus meets or exceeds the precision of the visual measurement procedure.

[4]Emergent properties arise out of more fundamental entities and yet are novel or irreducible with respect to them. [38]

At the stated non-relativistic velocity, the relativistic effects are not visible. However, if the velocity is increased by 2 orders of magnitude, from 0.00866c to 0.866c, then relativistic effects are observable, as is shown in the next section.

4.4.3 Classical Aberration

To demonstrate classic aberration, four depictions of the view of a distant object (star) were generated. The four positions on the Earth's orbit as shown in Figure 4.9 were chosen. The views from these four positions are displayed in Figures 4.10 and 4.11.

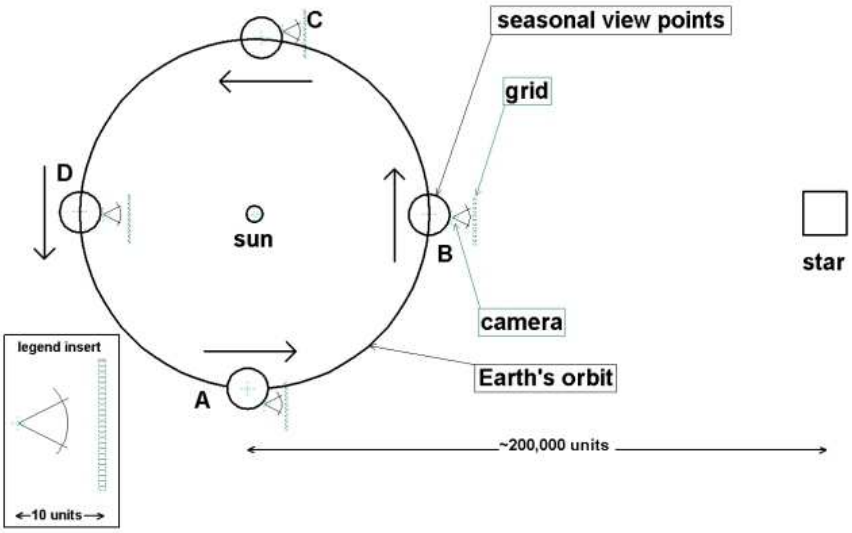

Figure 4.9: The four seasonal views from Earth
Earth's position in orbit with respect to cube (star) in Figures 4.10, 4.11 & 4.12.

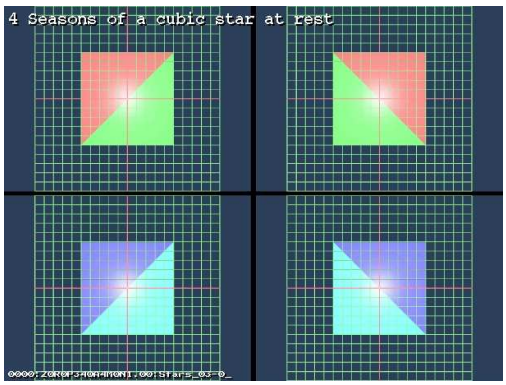

Figure 4.10: No Aberration - Observer at Rest

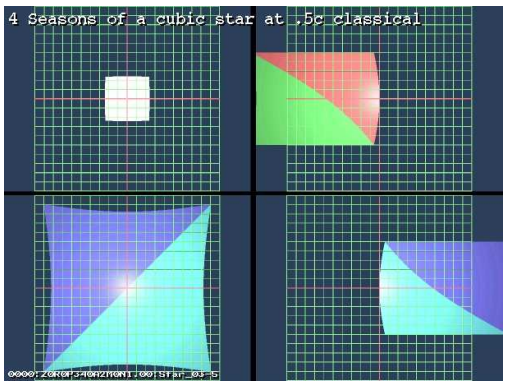

Figure 4.11: Classical Aberration Model at 0.500c

Figure 4.10 is a control-frame that depicts the cube (representing the star) from the four cardinal positions while at rest. Figure 4.11 shows the same four views of the cube, representative of the view of a star as seen from the Earth at three month intervals as it orbits

about the sun. Note that the cubes project onto the center of the reference grid 10 unit sides, as shown in each view from the observer at rest. Figure 4.9 depicts and Figure 4.11 shows, clockwise from the top left: (top left) the Earth approaching the star and the star's area compressing; (top right) the Earth moving to the left and the star migrating to the front of the moving Earth; (bottom right) the Earth moving to the right and the star migrating to the right; and (bottom left) the Earth moving away from the star and the star's image apparently expanding. The classical model will limit the aberration to less than 45 degrees, while the relativistic model in the next section, will allow the retreating star to envelop the entire visual sphere.

The cube is 1E5 units on a side, and lies 1.5E5 units from the observer (camera). The 20x20 grid lies between the cube and the observer 10 units from the observer. The cube and grid are positioned such that the cube (at rest) projects a 10x10 silhouette onto the grid centered on the red cross-hairs. So the cube at rest subtends an angle of arctan $\frac{10}{10}$ or 45° from the observer. Note that at 0.5c, the top right cube migrates approximately 26.6 degrees in the direction of motion of the observer with respect to the cube. This can be confirmed visually by noting that the right edge of the cube has move 5 grid marks left which equals arctan $\frac{5}{10} = 26.565°$.

4.4.4 Relativistic Aberration

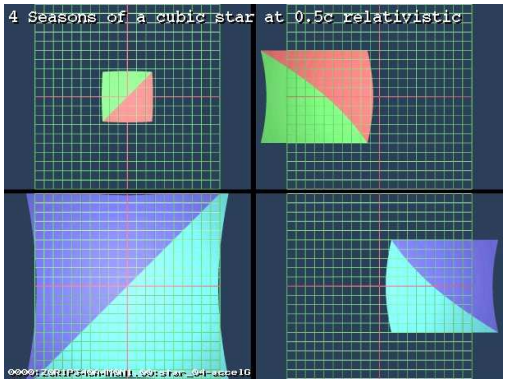

Figure 4.12: Relativistic Aberration Model at 0.500c

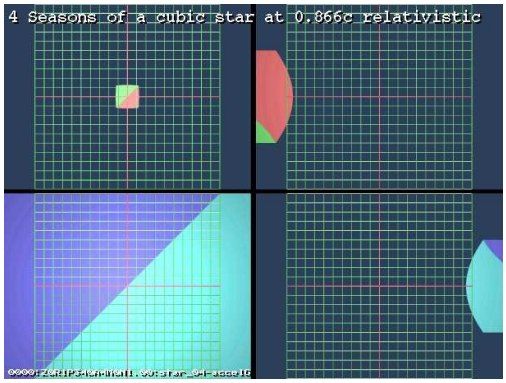

Figure 4.13: Relativistic Aberration Model at 0.866c

Relativistic aberration is likewise visualized with four views corresponding to views from four seasons of the Earth's orbit as depicted in Figure 4.9. The relativistic model introduces Lorentz length contraction of both the object, and the space in which the object is embedded. This leads to additional distortions in the object's geometry beyond those apparent for classical aberration, and will be obvious in the approach and retreat images.

Figure 4.12 shows four views of a cube, similar to that described in Section 4.4.3, Classical Aberration. As with the classical model, the cube at rest subtends an angle of arctan $\frac{10}{10}$ or 45° from the observer. Note that at 0.5c, the top right cube in Figure 4.12 migrates approximately 30° in the direction of motion of the observer with respect to the cube, slightly greater than the 26.565° of the Classical model in Figure 4.11. This can be confirmed visually by noting that the right edge of the top-right cube in Figure 4.12 has

moved 5.77 grid marks left which gives: arctan $\frac{5.77}{10} = 30.0°$; while in Figure 4.11 the right edge of the top-right cube has moved 5.00 grid marks to yield: arctan $\frac{5.00}{10} = 26.565°$.

The relativistic contribution is obvious in the leftmost two panels of Figure 4.12 showing approaching and retreating objects. While in the classical model, the lightspeed limits the angular distortion in a retreating view of an object to 45°, the relativistic model's angular aberration of an object trailing the observer can reach nearly 180°. The result is that at $0.866c$, the cube's edge moves from a position with respect to the direction of motion of 153.4° to 93.6°, effectively filling the panel, as shown in Figure 4.13.

4.4.5 Selected Animation Frames

Three models of relativistic motion are displayed in three rows of a sequence of five images from an animation in Figure 4.6. In all three rows the flanges (angle brackets) are moving at $0.866c$.

The finite lightspeed was decoupled from the physical effects in order to observe the respective contributions. Figure 4.6 depicts both decoupled finite lightspeed classical effects with no Lorentz transform and Lorentz transformed objects with relativistic effects. The images depict the ubiquitous flange approaching, crossing, and departing the centerline of the scene at $0.866c$. The top row of the image depicts an infinite lightspeed as per contemporary rendering, the middle row depicts a classical model of finite lightspeed with no physical effects, and the bottom row depicts the relativistic model showing the Lorentz contraction effects. The finite lightspeed camera was moved ahead in time (18.675 $t.units$), an amount equal to the lightspeed delay from the center of the stage to the camera, so that the flanges appear to be in approximately the same positions. The view in the top row would be impossible to capture from any camera position or camera inertial reference frame without computer graphics[5].

Note that the flanges in the bottom row *appear* to cross each other before the flanges in the top row. Note also, that even with this head start, the top flanges arrive at their respective stage edges at the same time as the bottom flanges. The bottom flanges appear to approach faster and retreat slower than the top flanges. This is the visual evidence of the classical aberration effect. The flanges approaching the centerline of the stage are effectively approaching the camera, which is relativistically equivalent to the camera approaching each of the individual flanges. This configuration causes the angle from the centerline to the flanges to appear smaller than the proper angle of incidence, so the object appears closer to the centerline, or ahead of the object's proper position as depicted in the top view, and as predicted by Equation (2.1).

This is true for both the leading and the trailing edges of the flange, independently. As a result, the leading edge, which is closer to the centerline, has seemed to move further than the trailing edge, giving the impression of a wider flange. The opposite effect occurs as the flanges move away from the centerline. The flanges appear to incrementally speed up and simultaneously contract as they move relativistically away from the camera. These aberration effects are apparent in the bottom two images of Figure 4.6.

[5]In reality, without computer visualization, the top views could only be physically captured from three separate cameras in three separate inertial reference frames and then matted together.

4.4.6 Terrell-Penrose-Boas Rotation

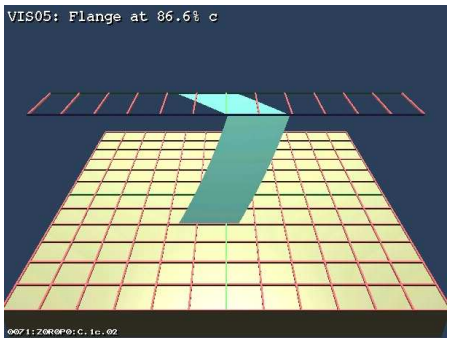

Figure 4.14: Terrell rotated flange (Lorentz decoupled)

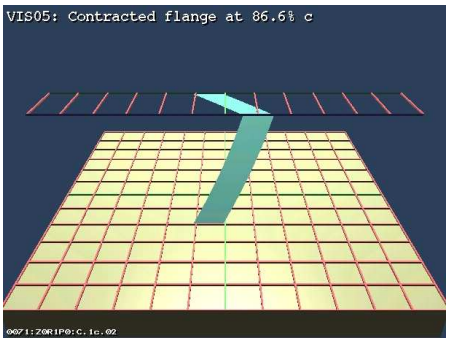

Figure 4.15: Terrell rotated and Lorentz contracted flange

Terrell and Penrose predicted that an object moving past an observer relativistically, would appear to rotate in the direction of motion. This effect can be seen clearly in Figure 4.15, where the flange is moving from left to right at $0.866c$. This is the same object, in the same position, as in Figure 4.14.

The classical distortion is an optical effect due to the finite limitation of the speed of light. The camera is at (0,9,15). As can be seen in Figure 4.14, when the flange's trailing edge is coincident with the $X = 0$ plane, the object's trailing upper left corner is at (0,4,2). This corner is then at a distance of [0,9,15] -[0,4,2] or 13.9 $l.unit$s from the camera. The trailing lower left corner is at (0,0,2), so the camera is at a distance of [0,9,15]-[0,0,2], or 15.8 $l.unit$s. Light will thus take 13.9 $t.unit$s to get to the camera from the first corner, and 15.8 $t.unit$s from the second corner, yielding a difference of 1.9 $t.unit$s. In 1.9 $t.unit$s, at 0.866c, the flange could travel 1.66 $l.unit$s, resulting in the trailing bottom edge of the flange being about 1.66 $l.unit$s behind the top trailing edge.

Careful examination of Figure 4.15 shows this to be the case, the apparent distance of the lower left corner of the flange from the green $x = 0$ gridline is about 1.66 $l.unit$s. Similarly the furthest top edge of the flange appears to coincidentally be trailing by the same distance behind the closest top edge. The overhead red rungs, between the green rails, are likewise spaced one $l.unit$ apart and can be used to reference the furthest top edge's trailing corner. This corner is at (0, 4, 0), and so is [0,9,15]-[0,4,0], or 15.8 $t.unit$ from the camera, the same as the trailing bottom corner. This coincidence was arranged by suitable placement of the camera, and demonstrates that the algorithm implemented in the VSTF is visibly accurate to within at least two decimal places.

Boas [10] predicted that straight lines would appear curved. This effect can be seen in the vertical edges of the flange in Figure 4.14. In addition, the masking of the Lorentz contraction is depicted in Figure 4.15. This is the same view as Figure 4.14, but with Lorentz contraction restored. As can be seen, the flange has contracted to exactly $\frac{1}{2}$ its proper length. Note also that the Terrell rotation has filled in for the contraction, thus masking the Lorentz contraction as predicted by Terrell.

Chapter 5

Discussion

5.1 Conclusions

Applying the principles of special relativity has yielded animation sequences of three-dimensional objects by four-dimensional raytracing of static three-manifolds embedded in a four-dimensional spacetime without modifying the three-dimensional scene between video-frames. The three-dimensional objects were extruded into a fourth dimension orthogonal to the three-dimensional axes. It was demonstrated that the apparent velocity of the animated object was related to the angle between the extrusion and this fourth axis. A raytracing engine was developed to intersect its rays with these four-dimensional objects from various points-of-view coincident with the fourth axis. It was demonstrated that if the point-of-view was advanced along this fourth axis, the objects appeared to move at velocities corresponding to the above described extrusion angle of the objects to this fourth axis. The objects exhibited characteristics attributed to objects moving with relativistic velocities with respect to the camera, such as Penrose-Terrell rotation, aberration and retarded position.

The Spacetime Raytracing strategy accurately renders objects with velocities from zero to the lightspeed-limit without modifying the object database between video-frames. The rendered image includes the usual photorealistic raytrace features such as reflection and shadows. Anti-aliasing can be extended into four-dimensions to provide motion-blur. The non-relativistic optical effects of relativistic velocities are intrinsic properties of the algorithm and naturally emerge as the object velocity with respect to the observer approaches the speed of light. Similar techniques could be applied to exploring the geometric properties of extra dimensions.

In conclusion, all relativistic visual phenomena ultimately can be modeled by two fundamental principles: finite lightspeed, a classical effect; and velocity (or τ-time) four-vector rotation in four-space, the relativistic effect. The latter is perceived as length-contraction and time-dilation in three-space. The resulting visual phenomena can be described in many ways, all correct, but not fundamental. Consequently, various superpositions of these visual phenomena are used to describe the fundamental principles.

5.2 Future Directions

The next generation of software should include the ability to specify accelerated object frames to enable the visualization of relativistically rotating bodies, as well as objects with curved worldlines. Also, heretofore non-geometric relativistic lighting effects including Doppler shift and the searchlight effect can be geometrized and demonstrated as yet another simple geometric effect.

Envisioned future software should also incorporate the ability to visualize extra spatial dimensions (beyond four dimensions). The term "*exotic physics*" refers to theories of physics that include extra dimensions. Likewise "exotic visualization" shall refer to the representation and visualization of extra spatial and time dimensions. The new software could thus visualize the Kaluza-Klein [31] [32] [2] five-dimensional spacetime, as well as other less well known five-dimensional and six-dimensional exotic physics models. The exploration of an extra time dimension will also be considered.

The most interesting bit of research thus lies ahead, specifically - the discovery of the n-dimensional geometric models that will allow the relativistic effects of length-contraction and time-dilation to emerge as did the classical optical effects of the model described here. The geometrization of τ-time four-vector rotation may be facilitated by the introduction of a fifth non-linear dimension. Other candidates for extra dimensional viewing also include the Arkani-Hamed, Dimopolous and Dvali large extra dimensions model [4], the Randall-Sundrum non-linear model [44], as well as the many Kaluza-Klein models [2], and other ***LXD*** models.

Other possibilities include visualizing electrodynamic interactions by tracing photon and particle paths. In like manner, gravitational interaction can be simulated via mediation by gravitons, whose behavior is similar to photons in certain toy-theories. It is not inconceivable that visualization at the quark and gluon level could likewise be explored with suitable modification of the software. The visualization and manipulation of the Schrödinger Wave Equation in four-dimensions is also intriguing. Since Lorentz-decoupling allows viewing of super-luminal velocities, an animation of the Alcubierre warp drive [1] is a possibility.

Bibliography

[1] Miguel Alcubierre. The warp drive: hyper-fast travel within general relativity. *arXiv.org e-Print archive, Class. Quant. Grav.*, 11:L73–L77, 1994.

[2] Thomas Appelquist, editor. *Modern Kaluza-Klein Theories*. Addison-Wesley Publishing Company, 1987. OUT OF PRINT. Pages 61-68, TH Kaluza, *On the unity problem in physics*, Pages 76-87, O. Klein, *Quantum theory and five dimensional theory of relativity*.

[3] George B. Arfken and Hans J. Weber. *Mathematical Methods for Physicists*. 2001.

[4] N. Arkani-Hamed, S. Dimopoulos, and G. Dvali. The hierarchy problem and new dimensions at a millimeter. *Phys. Lett. B*, 429:263, 1998.

[5] Werner Benger. Raytracing using hyperbolic light paths. In F.W.Hehl, R.A.Puntigam, and H.Ruder, editors, *Relativity and Scientific Computing*. Springer Verlag, Berlin Heidelberg New York, 1992.

[6] Don V Black. Realtime 4d hypercube viewing software. CALCOMP, Inc. Prisma Demo Utility, Sep 1985.

[7] Don V. Black. Raytracing special relativity with the searle backlight software package. http://www.HyperVisualization.com/videos/black, 2002.

[8] Don V. Black. Viewing classical and relativistic spacetime - accompanying animated videos. http://www.HyperVisualization.com/videos/black, 2004.

[9] Don V. Black. Spacetime visualization timeline. Technical Report ICS-TR-05-06, Dept. of Computer Science, University of California, Irvine, 2005.

[10] M. L. Boas. Apparent shape of large objects at relativistic speeds. *American Journal of Physics*, 29(5):283–286, May 1961.

[11] Max Born. *Einstein's Theory of Relativity*. Dover Publications, 1962, 1924. Chapter VI, Secton 4.

[12] M. F. Cohen and J. R.Wallace. *Radiosity and Realistic Image Synthesis*. Academic Press Professional, Boston, 1993.

[13] M. D'Zmura, P. Colantoni, and G. Seyranian. Virtual environments with four or more spatial dimensions. *Presence 9*, pages 616–631, 2001.

[14] M. D'Zmura and M. Ge. 4d structure from motion: a computational algorithm. *Computational Imaging (Proc SPIE/IS&T)*, 5016:13–23, 2003.

[15] Michael D'Zmura. The 4d web page, 2003. http://www.vrlab.uci.edu/dzmura/4D/.

[16] Michael D'Zmura. Navigation in 4-d virtual environments. Spring, 2005, 2005.

[17] Albert Einstein. On the electrodynamics of moving bodies. *Annalen der Physik*, (17):891–921, 1905.

[18] Albert Einstein. *Relativity, The Special and General Theory*. Pi Press, New York, 2005, 1916.

[19] Albert Einstein. *Relativity, The Special and General Theory*, chapter 16, Experience and the Special Theory of Relativity. Random House, Inc., New York, 1961, 1916.

[20] Albert Einstein. *Relativity, The Special and General Theory*, chapter Appendix 2, Minkowski's Four Dimensional Space ("World"). Random House, Inc., New York, 1961, 1916.

[21] Albert Einstein. *Relativity, The Special and General Theory*, chapter 17, Minkowski's Four Dimensional Space. Random House, Inc., New York, 1961, 1916.

[22] G. Gamow and R. Stannard. *The New World of Mr Tompkins*. University Press,Cambridge, 1999.

[23] Andrew S. Glassner. Spacetime raytracing for animation. *IEEE Computer Graphics and Applications*, 8(2):60–70, March 1988.

[24] Steven Richard Hollasch. Four-space visualization of 4d objects. Masters thesis, Arizona State University, 1991.

[25] P.-K. Hsiung and R. H. P. Dunn. Visualizing relativistic effects in spacetime. In *In Proceedings of Supercomputing,1989 Conference*, pages 597–606, 1989.

[26] P-K Hsiung and R.H. Thibadeau. Spacetime visualization of relativistic effects. In *Proceedings of the 1990 ACM annual conference on Cooperation*, pages 236–243, 1990.

[27] P-K Hsiung, R.H Thibadeau, C.B. Cox, and R.H.P Dunn. Time dilation visualization in relativity. In *Proceedings of Supercomputing November 1990*, pages 835–844, 1990.

[28] P-K Hsiung, R.H. Thibadeau, C.B. Cox, R.H.P. Dunn, M. Wu, and P.A. Olbrich. Wide-band relativistic doppler effect visualization. *Proceedings of the First IEEE Conference on Visualization, 1990*, pages 83–92, October 1990.

[29] P.-K. Hsiung, R.H. Thibadeau, and R.H.P. Dunn. Ray-tracing relativity. *ACM Pixel*, 1(1), 1990.

[30] P.-K. Hsiung, R.H. Thibadeau, and M. Wu. T-buffer: Fast visualization of relativistic effects in spacetime. In *Computer Graphics,1990 Symposium on Interactive 3D Graphics*, volume 24(2), pages 83–88. SIGGRAPH, ACM, 1990.

[31] T. Kaluza. On the unity problem of physics. *Physik.-Mathema Klasse*, pages 966–972, 1921.

[32] Oskar Klein. Quantum theory and five dimensional theory of relativity (1926). In Thomas Appelquist, editor, *Modern Kaluza-Klein Theories*. Addison-Wesley Publishing Company, 1987.

[33] Kenneth Krane. *Modern Physics*. John Wiley & Sons, 1996.

[34] C. Ernesto S. Lindgren and Steve M. Slaby. *Four-dimensional descriptive geometry*. McGraw-Hill Book Co., 1968.

[35] James Clerk Maxwell. *A Treatise on Electricity and Magnetism*. Clarendon Press, Oxford, 1873.

[36] H. Minkowski, H.A. Lorentz, A. Einstein, and H. Weyl. *The Principle of Relativity*, chapter V: H. Minkowski. Space and Time. Cologne, 1908. Dover Publications, 1923.

[37] G. Nordstrom. On the possibility of a unification of the electromagnetic and gravitation fields. *Physik Zeitschr*, 15:504–506, 1914.

[38] Timothy O'Connor and Hong Yu Wong. Emergent properties. In Edward N. Zalta, editor, *The Stanford Encyclopedia of Philosophy*. Stanford University, Summer 2005.

[39] Renato Pajarola, Yu Meng, and Miguel Sainz. Fast depth-image meshing and warping. Technical report, Technical Report UCI-ECE-02-02, The Henry Samueli School of Engineering, University of California Irvine, 2002.

[40] Wolfgang Pauli. *Theory of Relativity*. Pergamon Press, 1958. Page 17, Eqn (13).

[41] Roger Penrose. The apparent shape of a relativistically moving sphere. In *Proceedings of the Cambridge Philosophical Society*, volume 55, pages 137–139, 1959.

[42] Vesselin Petkov. *Relativity and the Nature of Spacetime*. Springer, 2005.

[43] Jules Henri Poincare'. *Analysis Situs*, volume 1. J. Ecole Polytechnique, 1895.

[44] L. Randall and R. Sundrum. A large mass hierarchy from a small extra dimension. *Phys. Rev. Lett.*, 83:3370, October 1999.

[45] R. Rau, D. Weiskopf, and H. Ruder. Special relativity in virtual reality. In *International Workshop on Visualization and Mathematics, VisMath '97*, 1997.

[46] Wolfgang Rindler. *Introduction to Special Relativity, 2nd Ed.* Oxford Science Publications, 1982. Eqns (13.3) & (18.2).

[47] Wolfgang Rindler. *Relativity: Special, General and Cosmological*. Oxford University Press, 2001. pages 81-82.

[48] Olaf Roemer. A demonstration concerning the speed of light. *Philosophical Transactions*, XII(136):893–894, June 1677.

[49] Antony C. Searle. Backlight ray tracer, 1997. http://www.anu.edu.au/Physics/Searle/.

[50] James Terrell. Invisibility of the lorentz contraction. *Physical Review*, 116(4):1041–1045, November 1959.

[51] D. Weiskopf. A texture mapping approach for the visualization of special relativity. In H. Hagen A. Varshney, C.M. Wittenbrink, editor, *IEEE Visualization '99 Late Breaking Hot Topics*, pages 41–44. ACM Press, October 1999.

[52] D. Weiskopf. Fast visualization of special relativistic effects on geometry and illumination. In R. van Liere W. de Leeuw, editor, *Proceedings of the EG/IEEE TCVG Symposium on Visualization*, pages 219–228. Springer, 2000.

[53] D. Weiskopf, U. Kraus, and H. Ruder. Searchlight and doppler effects in the visualization of special relativity: A corrected derivation of the transformation of radiance. *ACM Transactions of Graphics*, 18(3):278–292, July 1999.

[54] Daniel Weiskopf. daniel weiskopf - homepage. http://wwwvis.informatik.uni-stuttgart.de/ weiskopf/.

[55] Daniel Weiskopf. Institute for visualization and interactive systems, virtual reality software download, 1997. http://wwwvis.informatik.uni-stuttgart.de /eng/research/fields/current/relativity/specialrelativity/vr/vr-eng.html.

[56] Daniel Weiskopf. *Visualization of Four-Dimensional Spacetimes*. Ph.D. dissertation, University of Tübingen, 2001.

[57] Herbet G. Wells. *The Time Machine*. 1895.